Redox Biology 74 (2024) 103218

Contents lists available at ScienceDirect

Redox Biology

journal homepage: www.elsevier.com/locate/redox

ABCC1 deficiency potentiated noise-induced hearing loss in mice by impairing cochlear antioxidant capacity

Jing Liu [a,b,c,1], Yijiang Bai [a,b,c,1], Yong Feng [a,d], Xianlin Liu [a,b,c,e], Bo Pang [a,b,c,e], Shuai Zhang [a,b,c], Mengzhu Jiang [a,b,c], Anhai Chen [a,b,c], Huping Huang [a,b,c], Yongjia Chen [a,b,c], Jie Ling [f,**], Lingyun Mei [a,b,c,*]

[a] Department of Otolaryngology-Head and Neck Surgery, Xiangya Hospital, Central South University, Changsha, Hunan, China
[b] Otolaryngology Major Disease Research Key Laboratory of Hunan Province, Changsha, Hunan, China
[c] National Clinical Research Centre for Geriatric Disorders, Xiangya Hospital, Central South University, Changsha, Hunan, China
[d] Department of Otolaryngology-Head and Neck Surgery, The Affiliated Changsha Central Hospital, Hengyang Medical School, University of South China, Changsha, Hunan, China
[e] Hunan Key Laboratory of Medical Genetics, School of Life Sciences, Central South University, Changsha, Hunan, China
[f] Medical Functional Experiment Center, School of Basic Medical Science, Central South University, Changsha, Hunan, China

ARTICLE INFO

Keywords:
ABCC1 knockout
Noise-induced hearing loss
Stria vascularis
Oxidative stress
Glutathione

ABSTRACT

The *ABCC1* gene belongs to the ATP-binding cassette membrane transporter superfamily, which plays a crucial role in the efflux of various endogenous and exogenous substances. Mutations in *ABCC1* can result in autosomal dominant hearing loss. However, the specific roles of ABCC1 in auditory function are not fully understood. Through immunofluorescence, we found that ABCC1 was expressed in microvascular endothelial cells (ECs) of the stria vascularis (StV) in the murine cochlea. Then, an *Abcc1* knockout mouse model was established by using CRISPR/Cas9 technology to elucidate the role of ABCC1 in the inner ear. The ABR threshold did not significantly differ between WT and *Abcc1*$^{-/-}$ mice at any age studied. After noise exposure, the ABR thresholds of the WT and *Abcc1*$^{-/-}$ mice were significantly elevated. Interestingly, after 14 days of noise exposure, ABR thresholds largely returned to pre-exposure levels in WT mice but not in *Abcc1*$^{-/-}$ mice. Our subsequent experiments showed that microvascular integrity in the StV was compromised and that the number of outer hair cells and the number of ribbons were significantly decreased in the cochleae of *Abcc1*$^{-/-}$ mice post-exposure. Besides, the production of ROS and the accumulation of 4-HNE significantly increased. Furthermore, StV microvascular ECs were cultured to elucidate the role of ABCC1 in these cells under glucose oxidase challenge. Notably, 30 U/L glucose oxidase (GO) induced severe oxidative stress damage in *Abcc1*$^{-/-}$ cells. Compared with WT cells, the ROS and 4-HNE levels and the apoptotic rate were significantly elevated in *Abcc1*$^{-/-}$ cells. In addition, the reduced GSH/GSSG ratio was significantly decreased in *Abcc1*$^{-/-}$ cells after GO treatment. Taken together, *Abcc1*$^{-/-}$ mice are more susceptible to noise-induced hearing loss, possibly because ABCC1 knockdown compromises the GSH antioxidant system of StV ECs. The exogenous antioxidant *N*-acetylcysteine (NAC) may protect against oxidative damage in *Abcc1*$^{-/-}$ murine cochleae and ECs.

1. Introduction

Hearing loss is one of the most prevalent sensory disorders worldwide. According to statistics from the World Health Organization (WHO), the global population with hearing disabilities has reached 466 million, accounting for 6.1 % of the total world population (http://www.who.int). Hereditary hearing loss accounts for more than 60 % of hearing loss [1,2]. Most patients with autosomal dominant hearing loss exhibit delayed onset and experience a gradual progression of hearing loss, which can eventually lead to severe or profound hearing loss [3].

We previously reported that the *ABCC1* mutation was associated with autosomal dominant nonsyndromic hearing loss in a large Chinese family [4]. The protein ABCC1, also known as multidrug resistance

* Corresponding author.
** Corresponding author.
E-mail addresses: lingjie@sklmg.edu.cn (J. Ling), entmly@163.com (L. Mei).
[1] Jing Liu and Yijiang Bai contributed equally to this work.

https://doi.org/10.1016/j.redox.2024.103218
Received 7 March 2024; Received in revised form 14 May 2024; Accepted 28 May 2024
Available online 1 June 2024

Abbreviations

4-HNE	(4-hydroxy-2-nonenal glutathione conjugate)
ABCC1	(ATP-binding cassette membrane transporter superfamily 1)
ABR	(Auditory brainstem response)
CCK-8	(Cell Counting Kit-8)
DAPI	(4′,6-diamidino-2-phenylindole)
DHE	(Dihydroethidium)
EB	(Evans blue)
ECs	(Endothelial cells)
GO	(Glucose oxidase)
GSH	(Glutathione)
GSSG	(Oxidized glutathione)
IB4	(Isolectin B4)
IHCs	(Inner hair cells)
MCs	(Marginal cells)
MRP1	(Multidrug resistance protein 1)
NAC	(*N*-acetylcysteine)
NS	(Normal saline)
OHCs	(Outer hair cells)
PCR	(Polymerase chain reaction)
PFA	(paraformaldehyde)
PVM/Ms	(Perivascular-resident macrophage-like melanocytes)
ROS	(Reactive oxygen species)
SGNs	(Spiral Ganglion Neurons)
SPL	(Sound pressure level)
StV	(Stria vascularis)
vWF	(Von Willebrand Factor)
WT	(Wild type)

protein 1 (MRP1), is an ATP-binding cassette (ABC) transporter involved in contributing to multidrug resistance in some cancer cells, protecting certain tissues by outward transportation of various exogenous and endogenous toxic metabolites and regulating the leukotriene-mediated inflammatory response [5,6]. ABCC1 may also play a crucial role in mitigating the detrimental effects of oxidative stress, mainly because it mediates the efflux of glutathione (GSH), one of the most potent endogenous antioxidants, oxidized glutathione (GSSG),

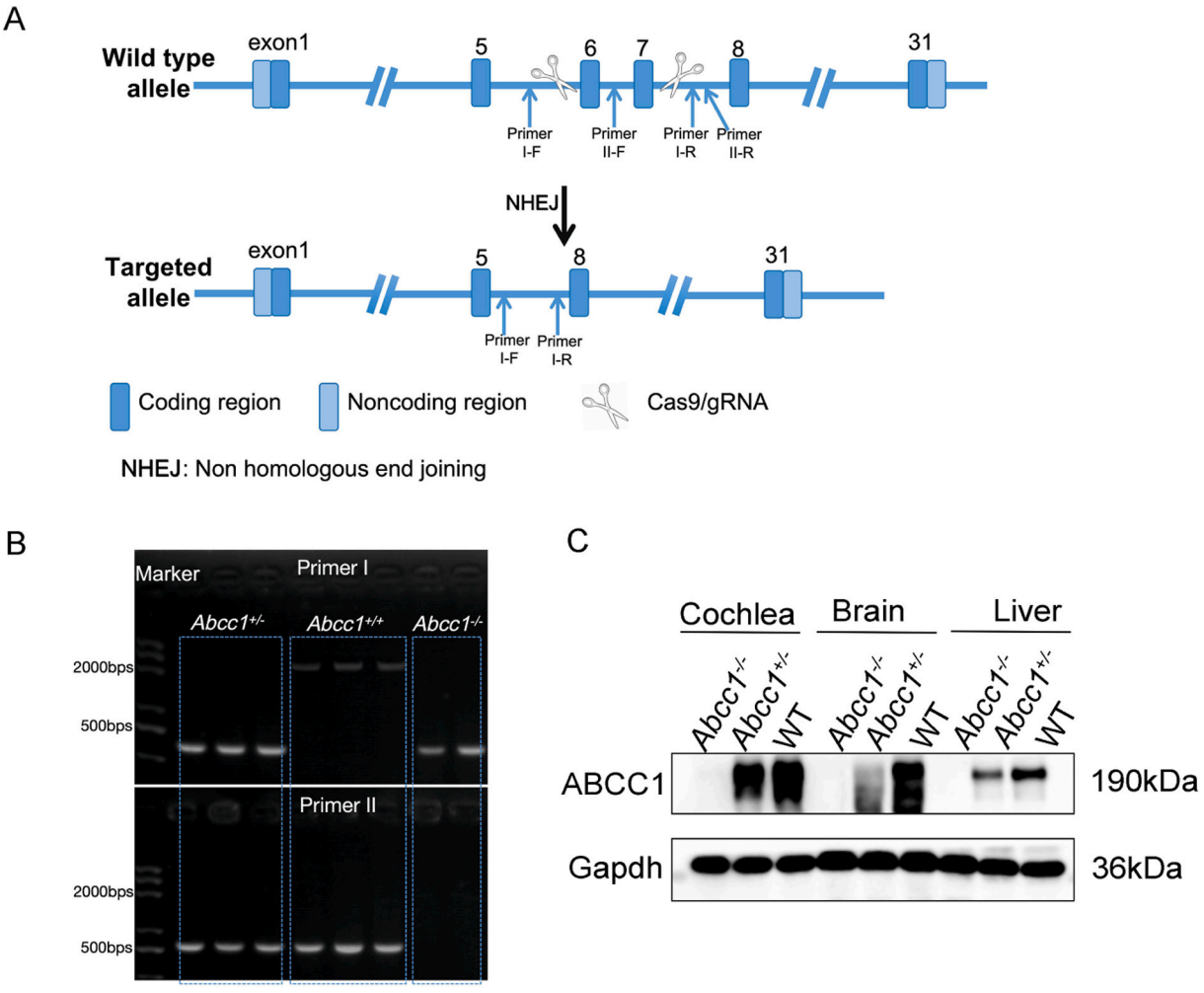

Fig. 1. Generation of C57BL/6Smoc-*Abcc1*^{em1Smoc} mice. (A) The murine *Abcc1* gene contains 31 exons, and the exons 6–7 were knockout using CRISPR/Cas9 technology. (B) PCR analysis for WT (lanes 4–6), *Abcc1*$^{+/-}$ (lanes 1–3) and *Abcc1*$^{-/-}$ (lanes 7 and 8) mice. For primer I, an expected band of 2320-bp was detected in WT mice; the 425-bp bands were detected in the *Abcc1*$^{+/-}$ and *Abcc1*$^{-/-}$ mice. For primer II, no band was detected in *Abcc1*$^{-/-}$ mice; and the 590-bp bands were detected in the WT and *Abcc1*$^{+/-}$ mice. (C) Western blot analysis revealed the protein expression levels of ABCC1 in the cochlea, brain, and liver following ABCC1 knockout.

4-hydroxy-2-nonenal glutathione conjugate (4-HNE), and other GSH-conjugated metabolites in various tissues [7–9].

ABCC1 is widely expressed in biological barriers, such as the blood–testis barrier, placental barrier and blood–brain barrier [10–12]. In the cochlea, Saito et al. first reported that ABCC1 was expressed in the stria vascularis (StV) and participated in the transportation of several chemotherapeutic drugs to avoid drug-induced ototoxicity [13]. As previously confirmed by our group, ABCC1 is located in the intermediate layer of the StV in the murine cochlea [4]. Intermediate cells mainly comprise perivascular-resident macrophage-like melanocytes (PVM/Ms) and endothelial cells (ECs), which construct the blood-labyrinth barrier and play an essential role in regulating the transport of inner ear substances and maintaining homeostasis in the inner ear [14]. However, the pathophysiological roles of ABCC1 in the inner ear and the mechanisms underlying its mutation-associated hearing loss remain unclear.

In this study, we confirmed the precise location of ABCC1 in the StV of the murine cochlea. Then, an *Abcc1* knockout mouse model was established using CRISPR/Cas9 technology to elucidate the role of ABCC1 in the murine inner ear under normal and noisy conditions. StV microvascular ECs were cultured from WT and *Abcc1*$^{-/-}$ murine cochleae to investigate the molecular changes associated with ABCC1 deficiency under oxidative stress in these cells.

2. Materials and methods

Ethical statement

The use of animals in this study and all the experiments were performed by the Animal Ethics Committee of the Institute of Xiangya Hospital, Central South University. We confirm that all the procedures were performed in accordance with the relevant rules.

2.1. Generation of Abcc1$^{-/-}$ *mice*

C57BL/6Smoc-*Abcc1*^{em1Smoc} mice were generated by Shanghai Model Organisms Center (Cat. NO. NM-KO-18012). Exons 6–7 of *Abcc1* were knockout using CRISPR/Cas9 technology in this mouse model (Fig. 1A). The mice were genotyped by polymerase chain reaction (PCR) using the following primers: primer I–F, 5′-GGGAGTGTAGATCAGTGAGG-3’; primer I–R, 5′-CACGGGAGCAGTCCCTGAAT-3’; primer II-F, 5′-CACTGTGACTGGTTCTGGTT-3’; and primer II-R, 5′-CCTACTTTGTCCCAATGCCT-3’ (Fig. 1B). Western blot analysis revealed that ABCC1 protein was successfully knockout in the cochleae, brains, and livers of *Abcc1*$^{-/-}$ mice compared to those of WT mice (Fig. 1C). Mice of both sexes were used. The animals were housed in the Laboratory Animal Facility at Central South University with the temperature maintained at 22 °C and a 12 h light/12 h dark-light cycle. The laboratory chow diet and sterilized water were provided ad libitum. The ambient noise around the mice was approximately 55 dB SPL.

2.2. Auditory brainstem response

ABR thresholds were recorded in mice after they were anesthetized with 375 mg/kg Avertin (Sigma, USA) and kept warm. To assess the effect of ABCC1 knockout on murine auditory function, the ABR thresholds of the mice were recorded at 2-month-old and 5-month-old. To assess the impact of noise exposure on murine auditory function, the ABR thresholds were recorded in mice before noise exposure and at 1 day and 2 weeks after noise exposure. Thresholds at click, 8, 16, 24, and 32 kHz were measured using a Tucker-Davis Technologies System workstation with SigGen32 software (Tucker-Davis Technologies Inc., Alachua, FL, USA). Stimulation was performed using a MF1 Multi-Field Magnetic Speakers (Tucker-Davis Technologies Inc., Alachua, FL, USA) calibrated with a sensor signal conditioner (model 480C02, PCB, NY, USA) and RZ6 Multi I/O Processor (Tucker-Davis Technologies Inc., Alachua, FL, USA). The live electrode was placed in the middle of the scalp, the ground electrode was placed in the shoulder blade on the back, and the reference electrode was placed under the skin of the test ear. The response was amplified 5020 times by a TDT Medusa4Z biological amplifier (bandpass filter: 30–3000 Hz, notch filter with 50 Hz), averaging 512 times. At each frequency, the sound level progressively decreases from 90 to 10 dB SPL. The ABR threshold is the lowest level defined to produce a significant ABR response.

2.3. Immunofluorescence

After the cochlea was removed, the tip of the cochlea was drilled and perfused with 4 % paraformaldehyde (PFA) and then fixed overnight with 4 % PFA at 4 °C. After decalcification with 10 % EDTA for 3 days, 7 μm thick frozen sections were obtained from the cochlea. Then, the sections were incubated with 0.5 % Triton X-100 (Sigma, USA) at room temperature for 15 min and blocked with 10 % goat serum at room temperature for 1 h. Then, the sections were incubated with monoclonal rabbit *anti*-ABCC1 antibody (Abcam, ab260038), polyclonal rabbit anti-4-HNE antibody (Alpha Diagnostic, HNE11-S), monoclonal rabbit *anti*-CtBP2 antibody (Abcam, ab128871), monoclonal rat *anti*-F4/80 antibody (Abcam, ab6640), or polyclonal rabbit anti-Von Willebrand Factor (vWF) antibody (Abcam, ab6994) at 4 °C overnight. The slides were subsequently washed three times with 0.01 M PBS. Then, the sections were incubated with goat anti-rabbit IgG H&L (Cy3®) (Abcam, ab6939), goat anti-rabbit IgG H&L (Alexa Fluor® 488) (Invitrogen, A11034), and goat anti-rat IgG H&L (Alexa Fluor® 568) (Abcam, ab175476) secondary antibodies for 1 h or with Phalloidin-iFluor 594 (Abcam, ab176757) for 30 min at room temperature under light-protected conditions. The nuclei were counterstained with 4’,6-diamidino-2-phenylindole (DAPI). Immunofluorescence images were taken with a confocal laser scanning microscope (Leica Microsystems).

2.4. Noise exposure and drug/placebo administration

Two-month-old mice in the experimental groups were placed in an anechoic chamber. After 1 day of environmental adaptation and acquisition of the baseline auditory brainstem, the mice were exposed to 80 dB SPL noise for 12 h per day for 7 consecutive days. The anechoic chamber has a loudspeaker (MS6520, JBL) mounted on the top. The speaker is driven by a TDT RZ6 multifunction processor and dedicated attenuator and controlled by TDT RPvdsEx sound processing software. The sound levels were calibrated with a sound meter (2550, Bruel & Kjær). The sound level was measured directly below the speaker at the height of the murine ear. The sound level at the edges of the cage was generally reduced by 1–3 dB. Individual cohorts of mice were intraperitoneally administered normal saline (NS) or 350 mg/kg NAC (S1623, Selleck) dissolved in NS. The administration commenced one day before noise exposure and continued for a duration of 7 days.

2.5. Evans blue (EB) infusions

The vessel integrity of the StV was determined by measuring EB extravasation. One hundred microliters of 2 % EB solution was intravenously administered via the tail vein. Two hours after infusion, the mice were perfused with 100 ml of NS and 100 ml of PFA. Then, the cochleae were dissected and fixed overnight with 4 % PFA at 4 °C. The StV was carefully dissected from the cochlea and tiled on glass slides. Fluorescence was detected under a confocal laser scanning microscope at an excitation wavelength of 594 nm. Evans blue leakage was measured using the fluorescence intensity of whole image, which included blood vessels.

2.6. DHE staining

Dihydroethidium (DHE), an ROS fluorescent probe, can freely

penetrate the cell membrane and be oxidized by intracellular ROS to form ethidium oxide. Ethidium oxide can be incorporated into chromosomal DNA to produce red fluorescence [15]. The cochleae were incubated with 1 μM DHE (Invitrogen, D23107) in 0.01 M PBS at 37 °C for 30 min and washed three times with 0.01 M PBS. Then, the cochlear specimens were perfused with 4 % PFA and fixed overnight with 4 % PFA at 4 °C, and 10 % EDTA was used for decalcification. The cochlear sections were isolated from the cochlea and sealed with an anti-fluorescent solution. A Leica laser confocal microscope was used to image the stained sections.

2.7. Primary culture of microvascular ECs from the StV

The procedure for preparing and primary culturing of microvascular ECs from the StV was described by Neng et al. [16]. In detail, WT and *Abcc1*$^{-/-}$ postnatal day 7 (P7) mouse pups were sacrificed, and the auditory bullae were rapidly separated and placed in a Petri dish with cold, fresh Hank's solution. Then, the StV was gently pulled away from the spiral ligament. After washing in fresh Hank's solution, the StV was transferred to an attachment factor (Gibco, USA)-coated 35 mm Petri dish with 2 ml of endothelial culture medium (ScienCell, USA) containing 5 % fetal bovine serum (Gibco, USA), 1 % endothelial cell growth factor (ScienCell, USA) and 1 % penicillin–streptomycin solution and cut into small pieces. Then, the fragmented pieces of StV were incubated in an incubator (37 °C, 5 % CO_2). The third to fifth passages of ECs were used.

To assess the purity of the ECs, the cells were resuspended and incubated with Isolectin B4 (IB4)-FITC conjugated (20 μg/ml) (Sigma–Aldrich, USA), an endothelial cell marker, for 30 min in the dark at 4 °C. Then, the cells were washed three times with 0.01 M PBS. The fluorescence signals were analyzed by fluorescence microscopy and flow cytometry.

2.8. Cell counting Kit-8 (CCK-8) assay

The viability of WT and *Abcc1*$^{-/-}$ ECs after oxidative stress challenge was measured by a CCK-8 assay (APExBIO, Texas, USA) according to the manufacturer's protocol. Briefly, WT and *Abcc1*$^{-/-}$ cells were resuspended, and 1×10^4 cells/well were seeded into 96-well plates. The next day, the WT and *Abcc1*$^{-/-}$ cells were treated with 0, 10, 20, 30, 40, 50, 60, 70 or 80 U/L GO (Sigma–Aldrich, USA) or 0 U/L GO, 10 mM NAC, 30 U/L GO or 30 U/L GO + 10 mM NAC for 4 h, and each treatment was tested in triplicate. To determine the viability of the cells, 10 μl of CCK-8 test solution was added to each well and incubated for another 2 h. After that, the cell viability was determined by the absorbance at 450 nm using a microplate reader.

2.9. Measurement of reactive oxygen species (ROS) production

WT and *Abcc1*$^{-/-}$ cells were resuspended, and 2×10^5 cells/well were seeded into 6-well plates. The next day, the WT and *Abcc1*$^{-/-}$ cells were treated with 0, 10, 30 or 80 U/L GO or 0 U/L GO, 10 mM NAC, 30 U/L GO or 30 U/L GO + 10 mM NAC for 4 h. After treatment, the cells were harvested and incubated with 100 μM DHE for 30 min in the dark at 37 °C. Then, the cells were washed three times with 0.01 M PBS. The fluorescence signals were analyzed by flow cytometry.

2.10. Annexin V/PI double staining

WT and *Abcc1*$^{-/-}$ cells were resuspended, and 2×10^5 cells/well were seeded into 6-well plates. The next day, the WT and *Abcc1*$^{-/-}$ cells were treated with 0, 10, 30 or 80 U/L GO or 0 U/L GO, 10 mM NAC, 30 U/L GO or 30 U/L GO + 10 mM NAC for 4 h. After treatment, the cells were harvested, washed three times with 1 × binding buffer and then incubated in 1 × binding buffer supplemented with 5 % FITC-Annexin V and 10 % PI (Yeasen, China) for 15 min in the dark at room temperature. Then, the cells were resuspended in cold and fresh 1X binding buffer and analyzed by flow cytometry.

2.11. GSH/GSSG assay

WT and *Abcc1*$^{-/-}$ cells were resuspended, and 2×10^5 cells/well were seeded into 6-well plates. The next day, the WT and *Abcc1*$^{-/-}$ cells were treated with 0, 10, 30 or 80 U/L GO for 4 h. After treatment, the concentrations of total glutathione (GSH) and oxidized GSH (GSSG) in treated cells were measured using GSH and GSSG assay kits (Beyotime, China) according to the manufacturer's protocol. Then, the concentrations of reduced GSH and the ratio of reduced GSH/GSSG were calculated according to the manufacturer's protocol (reduced GSH = total glutathione- 2× GSSG).

2.12. Western blot

The mice were deeply anesthetized, and the cochlea was promptly removed from the skull. Subsequently, the samples were rinsed with cold 10 mM PBS (pH 7.4) and thoroughly homogenized using a grinding rod in RIPA lysis buffer supplemented with protease inhibitors (APExBIO, K1007, diluted at a ratio of 1:100). Following centrifugation at 13,000 rpm for 15 min at 4 °C, the supernatant was collected. WT and *Abcc1*$^{-/-}$ cells were resuspended for the experiments with primary cultured cells, and 4×10^5 cells/well were seeded into 6-well plates. The next day, the WT and *Abcc1*$^{-/-}$ cells were treated with 0, 10, 30 or 80 U/L GO or 0 U/L GO, 10 mM NAC, 30 U/L GO or 30 U/L GO + 10 mM NAC for 4 h. After treatment, the total proteins of the treated cells were extracted using RIPA lysis buffer with protease inhibitor cocktail, and the nuclear and cytoplasmic extracts were prepared using an NE-PER™ nuclear and cytoplasmic extract reagent kit following the manufacturer's protocol. Ten micrograms of protein extract per sample was mixed with protein loading buffer (Yessen, China), separated on SDS–polyacrylamide gels, and transferred onto polyvinylidene difluoride membranes. The membranes were blocked in TBST containing 5 % skim milk for 1 h and incubated with primary antibodies overnight at 4 °C. After washing with TBST three times, the membranes were incubated with HRP-conjugated secondary antibodies at room temperature for 1 h. Then, the protein bands were detected using an enhanced ECL reagent (Zen Bioscience, China) from Azure Biosystems C300 (Azure Biotech, USA). The following antibodies were used: rabbit anti-4-HNE antibody (1:1000, Alpha Diagnostic, USA), rabbit *anti*-GPX4 antibody (1:1000, Abmart, China), rabbit *anti*-KEAP1 antibody (1:1000, HuaBio, China), rabbit *anti*-NRF2 antibody (1:1000, Proteintech, China), rabbit *anti*-Lamin B1 antibody (1:1000, HuaBio, China), rabbit anti–HO–1 antibody (1:5000, Abcam, USA), mouse *anti*-GAPDH antibody (1:5000, Zen Bioscience, China), goat anti-rabbit IgG (H + L)-HRP (1:10,000, Abcam, USA), and goat anti-mouse IgG (H + L)-HRP (1:10,000, Abcam, USA).

2.13. Cell counting and statistical analysis

To quantify the survival rate of hair cells, three segments obtained from the apical turn, middle turn and basal turn were selected from the tip to the bottom of the cochlea, and immunostained positive cells were counted. The data are expressed as the mean ± SD. A *t*-test was used to analyze the differences between the two groups. Differences between groups were compared using one-way ANOVA and a Bonferroni post hoc correction for multiple comparisons. For comparisons of differences in other data between three or more groups, multiple comparisons were performed using two-way ANOVA and the Bonferroni post hoc correction. P values less than 0.05 were considered to indicate statistical significance.

3. Results

3.1. ABCC1 was expressed in microvascular ECs of the StV

Consistent with our previous findings, ABCC1 was expressed in the intermediate layer of the StV in the murine cochlea at different developmental stages (Fig. 2A(a, b)) [4]. Since the intermediate layer of StV comprises several types of cells, we further identified the precise location of ABCC1 in 2-month-old murine StV through immunofluorescence. As shown in Fig. 2A(c-e, i-l), ABCC1 colocalized with vWF, which is an endothelial cell marker. Furthermore, ABCC1 was not expressed in perivascular resident macrophage-type melanocytes labeled with F4/80 (Fig. 2A(f-h)). These results indicated that ABCC1 was specifically expressed in microvascular ECs within the StV and may play a critical role in the cochlea.

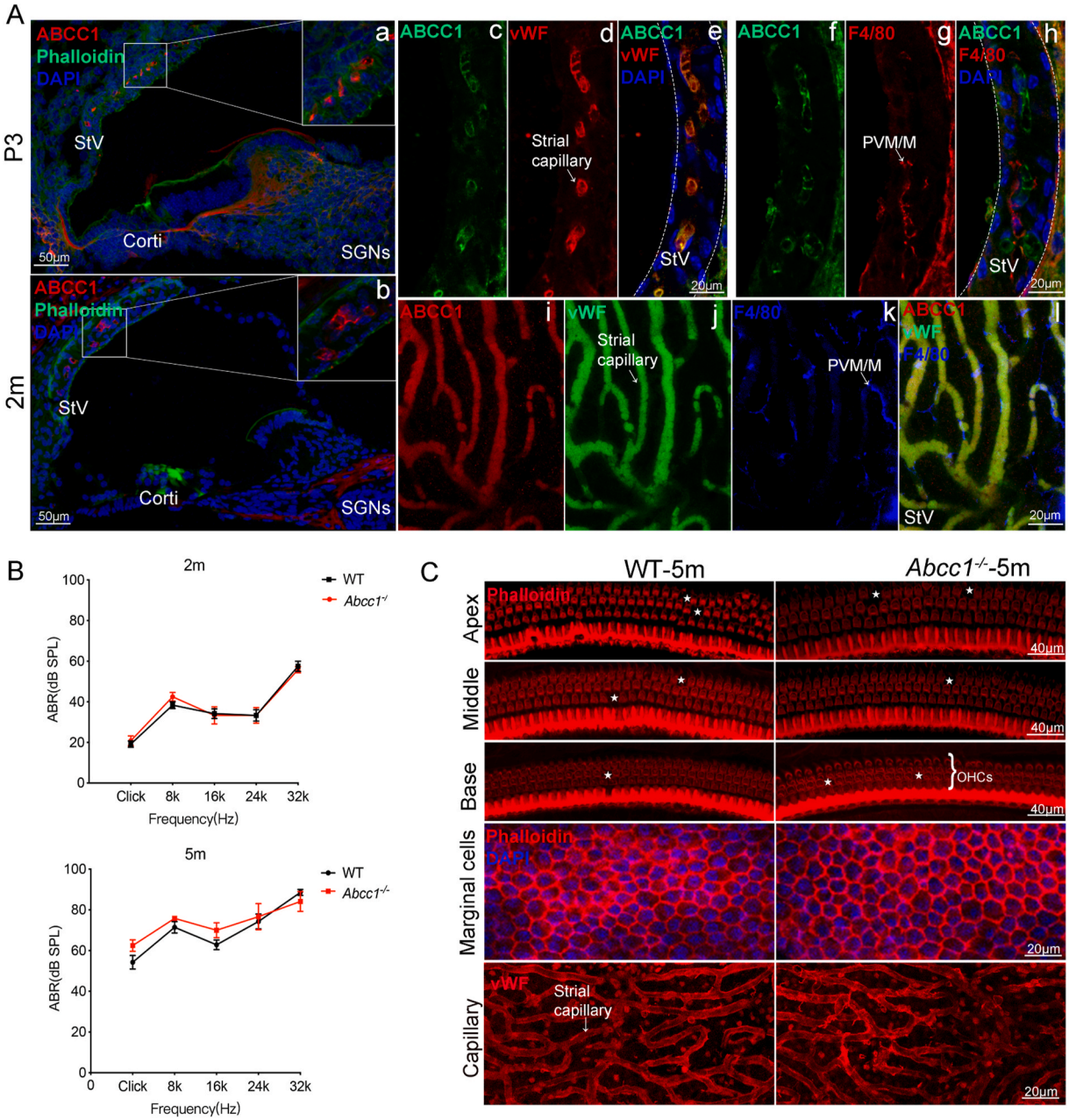

Fig. 2. ABCC1 was expressed in microvascular ECs in the stria vascularis of the cochlea, and *Abcc1*$^{-/-}$ mice exhibited normal cochlear development and hearing function. (A) ABCC1 immunofluorescence staining in the cochleae. (a, b) Frozen sections of P3 and P60 mouse cochleae showing ABCC1 (red) distributed in the intermediate layer of the StV. Sections were counterstained with DAPI (blue) to identify nuclei. Scale bar: 50 μm. (c–e) The frozen sections of P60 mouse cochleae exhibited colocalization of ABCC1 (green) and vWF (red). Scale bar: 20 μm. (f–h) No colocalization of ABCC1 (green) and F4/80 (red) was detected. (e, h) The white dashed line delineates the outline of the StV. (i–l) The expression of ABCC1 (red) was further examined through immunofluorescence in whole mounts of the StV. vWF labeled vascular endothelial cells; F4/80 labeled PVM/M; PVM/M: perivascular melanocytic macrophage-like cell; StV: stria vascularis; Corti: organ of Corti; SGNs: spiral ganglion neurons. Scale bar: 20 μm. (B) ABR thresholds of 2-month-old WT and *Abcc1*$^{-/-}$ mice (n = 10 for each group). (C) Confocal images showing the whole mounts of organ of Corti and the marginal and intermediate layers of the StV in WT and *Abcc1*$^{-/-}$ mice. The white pentagrams indicate the absence of OHCs. The scale bar for the organ of Corti: 40 μm; the scale bar for the StV: 20 μm. OHCs: outer hair cells. (For interpretation of the references to colour in this figure legend, the reader is referred to the Web version of this article.)

3.2. *Abcc1*$^{-/-}$ mice had normal hearing function and cochlear structure

To evaluate the impact of ABCC1 knockout on auditory function, we successively detected the ABR threshold of *Abcc1*$^{-/-}$ mice until 5 months of age. There were no significant differences in the ABR threshold between WT mice (n = 10) and *Abcc1*$^{-/-}$ mice (n = 10) at 2 and 5 months of age (Fig. 2B). Immunofluorescence images revealed that compared with WT mice, *Abcc1*$^{-/-}$ mice exhibited no obvious morphological changes in the StV, sensory hair cells or SGNs (Fig. 2C). Taken together, these findings indicate that the auditory function of *Abcc1*$^{-/-}$ mice was not compromised under normal conditions at least up to the oldest age studied, 5 months. This result indicated that ABCC1 mutation-induced hearing loss may involve a complex interplay between the environment and genetics.

3.3. *Abcc1*$^{-/-}$ mice hardly recovered from noise-induced hearing loss

Further investigation of the previous ABCC1 mutant family revealed that this family was exposed to more noise at work and in life [4]. Therefore, to investigate whether ABCC1 mutation-induced hearing loss was associated with noise exposure, WT and *Abcc1*$^{-/-}$ mice were exposed to 80 dB SPL noise conditions for 1 week (Fig. 3A). Before noise exposure, the ABR threshold did not obviously differ between WT and *Abcc1*$^{-/-}$ mice (Fig. 3B and C). One day after noise exposure, the ABR thresholds of the WT and *Abcc1*$^{-/-}$ mice were significantly elevated (Fig. 3B and C). Interestingly, the ABR threshold of the WT mice returned to baseline after 14 days of recovery, while the ABR threshold of the *Abcc1*$^{-/-}$ mice did not change between 1 day and 14 days after noise exposure recovery (Fig. 3B and C).

EB can bind to serum albumin immediately following intravenous injection and exhibits red fluorescence [17]. The vessel integrity of the StV in WT and *Abcc1*$^{-/-}$ mice was assessed through EB infusions. Before noise exposure, EB was barely detectable in the vascular lumen of the StV in WT and *Abcc1*$^{-/-}$ mice. However, 14 days after noise exposure, EB entered the perivascular interstices of the StV in the WT and *Abcc1*$^{-/-}$ mice, and the fluorescence intensity of EB was significantly greater in the *Abcc1*$^{-/-}$ murine StV (Fig. 3D–F). This result indicated that vessel leakage was more severe in *Abcc1*$^{-/-}$ murine StV after noise exposure.

Furthermore, morphological changes in the organ of Corti were tested in *Abcc1*$^{-/-}$ mice after 14 days of recovery. Although the inner hair cells (IHCs) remained intact, the number of OHCs in the *Abcc1*$^{-/-}$ mice was significantly lower than that in the WT mice (Fig. 3G and H). In addition, the number of ribbons was significantly decreased in the cochleae of *Abcc1*$^{-/-}$ mice (Fig. 3I and J). In summary, the auditory function of *Abcc1*$^{-/-}$ mice was more susceptible to noise-induced hearing loss. These morphological changes indicated that noise exposure may result in a permanent threshold shift in *Abcc1*$^{-/-}$ mice.

3.4. Oxidative stress products accumulated in the cochleae of *Abcc1*$^{-/-}$ mice after noise exposure

Since oxidative stress plays a major role in noise-induced hearing loss [18], we further detected oxidative stress products in the cochleae of *Abcc1*$^{-/-}$ mice 14 days after noise exposure. Immunofluorescence images revealed that reactive oxygen species (ROS) accumulated mainly in the StV, sensory hair cells and spiral ganglion neurons (Fig. 4). Before noise exposure, there were no significant differences in the immunofluorescence intensities of DHE and 4-HNE, an oxidative product, between the WT and *Abcc1*$^{-/-}$ groups (Fig. 4A–D). Compared to those in WT mice, the fluorescence intensities of DHE and 4-HNE were significantly greater in the cochleae of *Abcc1*$^{-/-}$ mice (Fig. 4A–D). Moreover, the expression of 4-HNE was significantly increased in the cochleae of *Abcc1*$^{-/-}$ mice (Fig. 4E and F). These results indicated that the compromised auditory function in *Abcc1*$^{-/-}$ mice may be linked to excessive oxidative stress after noise exposure.

3.5. *Abcc1*$^{-/-}$ ECs are more susceptible to GO-induced oxidative stress

To further investigate the specific role of ABCC1 in the cochlea under oxidative stress, we cultured StV microvascular ECs from WT and *Abcc1*$^{-/-}$ mice (Fig. S1). Primary ECs climbed out from the tissue block and gradually formed a “paved stone” monolayer, which is typical of endothelial cell morphology (Fig. S1A). IB4, a specific endothelial cell marker, was used to identify endothelial cells among primary cultured cells [16]. Through flow cytometry analysis, more than 90 % of the primary cultured cells were IB4 positive cells (Fig. S1B).

ABCC1 deficiency had no apparent adverse effect on the viability of ECs under standard culture conditions. GO can continuously generate hydrogen peroxide to induce oxidative stress [19]. After GO treatment, the viability of the WT and *Abcc1*$^{-/-}$ cells decreased in a concentration-dependent manner. GO concentrations exceeding 20 U/L significantly decreased the viability of WT and *Abcc1*$^{-/-}$ cells, and this effect was further enhanced by ABCC1 knockout (Fig. S2). In subsequent experiments, the cells were treated with 0, 10, 30 or 80 U/L (representing the control group, low, intermediate and high concentration groups, respectively) GO for 4 h to investigate the molecular changes between the WT and *Abcc1*$^{-/-}$ cells.

After 0 and 10 U/L GO treatment, the intracellular ROS levels, 4-HNE levels and apoptotic rates were not significantly different between the WT and *Abcc1*$^{-/-}$ cells (Fig. 5A–F). Compared with those in the 0 U/L GO treated control group, only the 80 U/L GO treatment significantly increased the intracellular ROS levels and apoptotic rates in the WT cells (Fig. 5A, B, E, F). In *Abcc1*$^{-/-}$ cells, compared with those in the 0 U/L GO treated control group, intracellular ROS levels and apoptotic rates were significantly elevated after 30 and 80 U/L GO treatment (Fig. 5A, B, E, F). Compared with those in WT cells, the intracellular ROS levels, 4-HNE levels and apoptotic rates were significantly greater in *Abcc1*$^{-/-}$ cells after 30 U/L GO treatment (Fig. 5A–F). Taken together, these findings indicate that primary cultured StV microvascular ECs are more susceptible to GO-induced oxidative stress damage.

3.6. ABCC1 knockout compromised the antioxidant capacity of ECs

We further examined the impact of ABCC1 deficiency on endogenous antioxidants under oxidative stress. GSH is a major endogenous antioxidant, and its metabolites can be directly transported by ABCC1 [7, 20]. GSH and GSSG levels did not change in *Abcc1*$^{-/-}$ cells without GO challenge. After 30 U/L GO treatment, the intracellular GSH and GSSG levels were barely changed in the WT cells (Fig. 6A). Nevertheless, in *Abcc1*$^{-/-}$ cells, the reduced GSH/GSSG ratio was significantly decreased after 30 U/L GO treatment. Compared with those in WT cells, although total GSH and reduced GSH levels were barely changed, the GSSG levels in *Abcc1*$^{-/-}$ cells were significantly greater than those in WT cells, leading to a marked decrease in the reduced GSH/GSSG ratio after 30 U/L GO treatment (Fig. 6A). After 80 U/L GO treatment, the total GSH levels, reduced GSH levels and reduced GSH/GSSG ratio were significantly decreased, while the GSSG levels were elevated significantly in the WT and *Abcc1*$^{-/-}$ cells (Fig. 6A).

Next, we investigated the NRF2/HO-1/GPX4 signaling pathway, which is a main signaling pathway that protects various cells and tissues against oxidative stress [21]. In *Abcc1*$^{-/-}$ cells, the expression of KEAP1 was significantly decreased, and the expression of nuclear NRF2 was significantly increased after 10 U/L and 30 U/L GO treatment (Fig. 6B, C, F, G). In addition, after 30 and 80 U/L GO treatment, the expression of KEAP1 and GPX4 significantly decreased, while the expression of HO-1 significantly increased (Fig. 6B–E). Compared with WT cells, *Abcc1*$^{-/-}$ cells showed changes in the expression of KEAP1 and nuclear NRF2 after 10 U/L GO treatment (Fig. 6B, C, F, G). These results indicate that *Abcc1*$^{-/-}$ cells may need to recruit the NRF2 signaling pathway to protect against low doses of oxidative stress, which is not a cytotoxic dose for WT cells. In addition, after 30 U/L GO treatment, the expression of cytosolic NRF2 did not change, yet the levels of nuclear NRF2 and

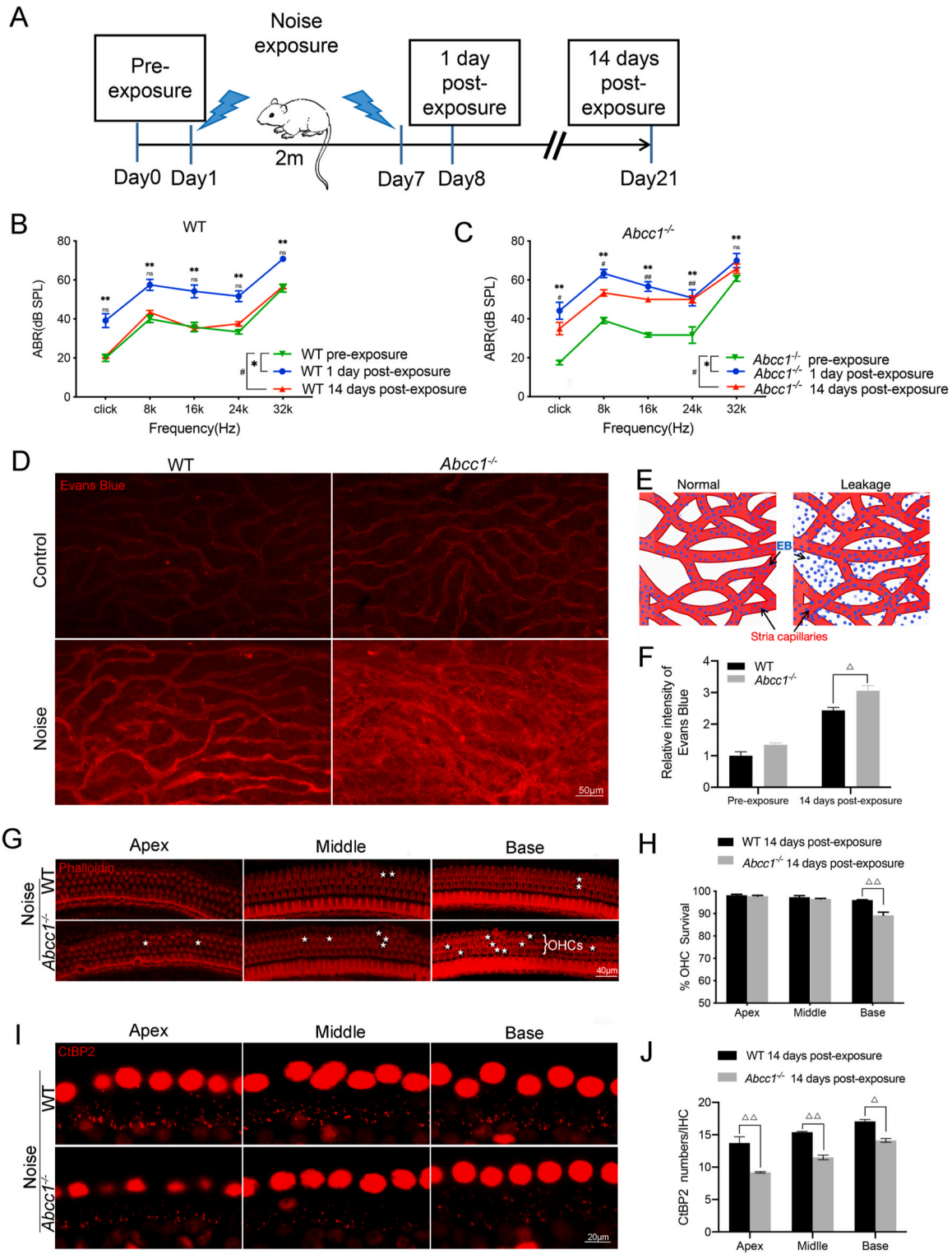

Fig. 3. ABR threshold shifts and morphological changes in OHCs and ribbons in WT and *Abcc1*$^{-/-}$ mice following noise exposure. (A) Experimental design for noise exposure. Two-month-old WT and *Abcc1*$^{-/-}$ mice were used. The ABR thresholds of WT and *Abcc1*$^{-/-}$ mice were tested pre-exposure and at 1 day and 14 days post-exposure (n = 6 for each group). (B–C) ABR thresholds of WT and *Abcc1*$^{-/-}$ mice before and after noise exposure (n = 6 for each group). (D) Confocal images of microvessels in the StV 2 h after EB infusion. Evans blue was injected into the mice before and 14 days after noise exposure. (E) Schematic representation of blood vessel leakage. (F) The bar graph showed the quantification of EB intensity (n = 3 for each group). (G) Confocal images of the organ of Corti in the WT and *Abcc1*$^{-/-}$ mice 14 days post-exposure. The white pentagrams indicate the absence of OHCs. Scale bar: 40 μm. (H) Percentage of OHC loss at different cochlear locations in WT and *Abcc1*$^{-/-}$ mice (n = 5 for each group). (I) Confocal images of ribbons in WT and *Abcc1*$^{-/-}$ mice 14 days after noise exposure. Scale bar: 20 μm. (J) Number of ribbons per IHC at different cochlear locations in WT and *Abcc1*$^{-/-}$ mice (n = 5 for each group). Comparison of pre-exposure and 14 days post-exposure: ns $P \geq 0.05$, #$P < 0.05$, ##$P < 0.01$. Comparison of 1 day post-exposure and 14 days post-exposure: *$P < 0.05$, **$P < 0.01$. Comparison of the WT and *Abcc1*$^{-/-}$ groups 14 days after exposure: Δ $P < 0.05$, ΔΔ $P < 0.01$. (For interpretation of the references to colour in this figure legend, the reader is referred to the Web version of this article.)

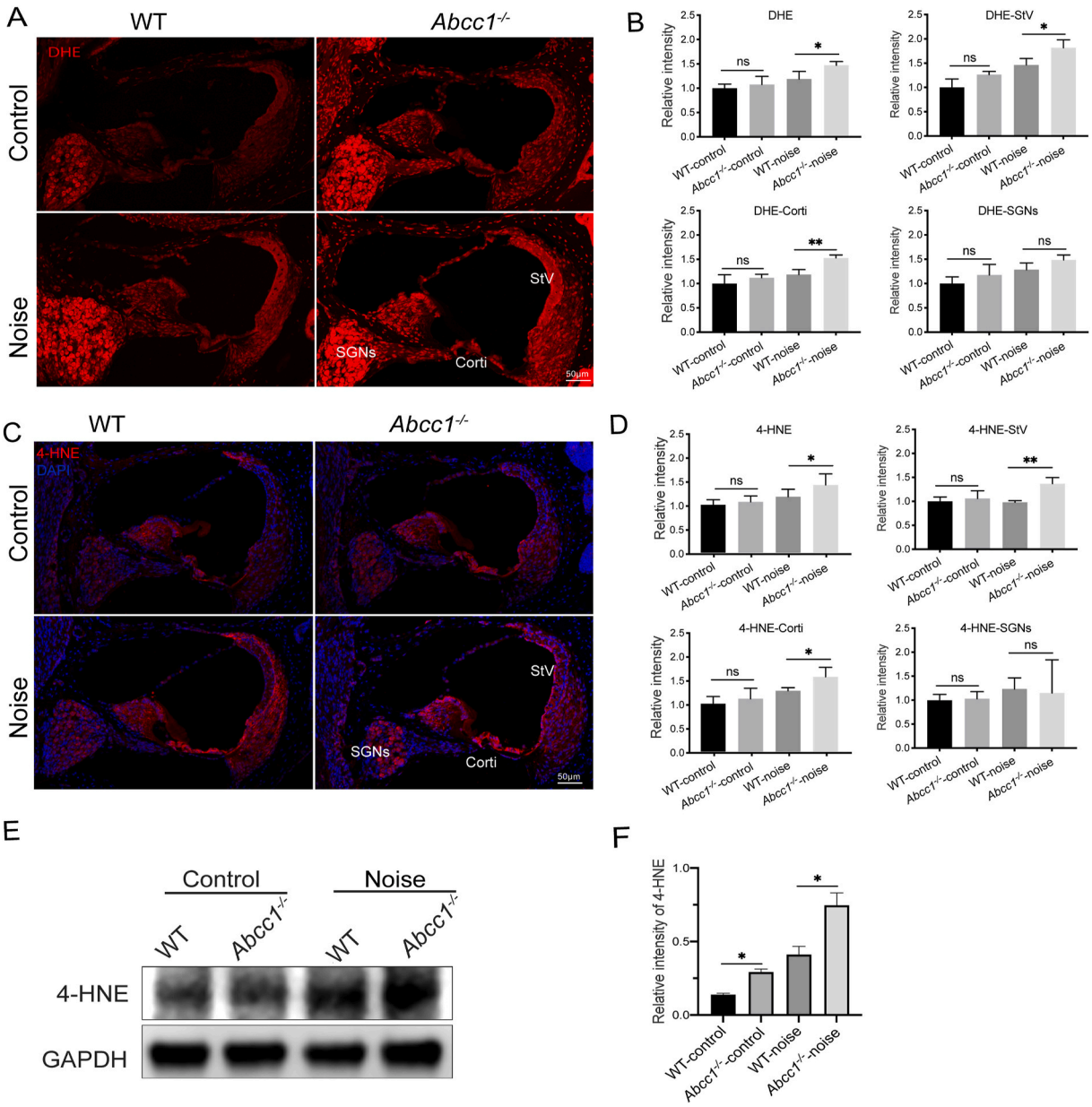

Fig. 4. Noise induced oxidative stress and 4-HNE accumulation in the inner ears of *Abcc1*$^{-/-}$ mice. (A, C) Representative confocal images of cryosections (10 μm) of the cochlea showing enhanced DHE (A) and 4-HNE (C) fluorescence signals of the organ of Corti, SGN, and StV within the *Abcc1*$^{-/-}$ cochlea. StV: stria vascularis; Corti: organ of Corti; SGNs: spiral ganglion neurons. (B, D) Quantification of the fluorescence signals of DHE and 4-HNE in different parts of the cochlea (organ of Corti, StV, and SGNs) as measured by optical density (data normalized to the control) (n = 3 for each group). 14 days after noise exposure, the immunofluorescence intensities of both DHE and 4-HNE were significantly greater in most of the cochlear structures of the *Abcc1*$^{-/-}$ mice than in those of the WT mice. Scale bar: 50 μm. (D, E, F) Western blotting and densitometric analysis of 4-HNE in cochlear tissue homogenates from WT and *Abcc1*$^{-/-}$ mice (n = 3 for each group). GAPDH served as a loading control for 4-HNE. Compared with WT group, expression of 4-HNE in *Abcc1*$^{-/-}$ groups was significantly increased in both of before exposure and 14 days after exposure. Comparison of the WT and *Abcc1*$^{-/-}$ groups under the same treatment conditions: ns $P \geq 0.05$, *$P < 0.05$, **$P < 0.01$.

HO-1 in *Abcc1*$^{-/-}$ cells were significantly greater than those in WT cells (Fig. 6B, *E*-H). This indicates that the NRF2 signaling pathway was more active in *Abcc1*$^{-/-}$ cells.

Overall, we speculated that the loss of ABCC1 in ECs may compromise the GSH antioxidant system, leading to decreased antioxidant capacity in *Abcc1*$^{-/-}$ cells after GO treatment (Fig. 6I and J).

3.7. Treatment with NAC alleviated oxidative stress damage in *Abcc1*$^{-/-}$ mice and ECs

NAC is a potent glutathione precursor that increases intracellular glutathione levels after its entry into cells [22]. Our data showed that after 7 consecutive days of NAC administration, noise-induced hearing loss was mitigated in *Abcc1*$^{-/-}$ mice. After 14 days of recovery, there was no obvious threshold shift in the WT mice. Compared with those in the NS treated group, the ABR thresholds of the *Abcc1*$^{-/-}$ mice in the NAC treated group were significantly lower. (Fig. 7A and B). Consistently, the fluorescence intensity of EB in the StV of *Abcc1*$^{-/-}$ mice was significantly reduced in the NAC treated group (Fig. 7C and D). In addition, the damage to OHCs and ribbons in *Abcc1*$^{-/-}$ mice was significantly alleviated in the NAC treated group (Fig. 7*E*–H).

We further investigated the protective role of NAC in *Abcc1*$^{-/-}$ ECs. NAC treatment significantly increased the viability of primary cultured WT and *Abcc1*$^{-/-}$ cells after 30 U/L GO treatment (Fig. S3). In addition,

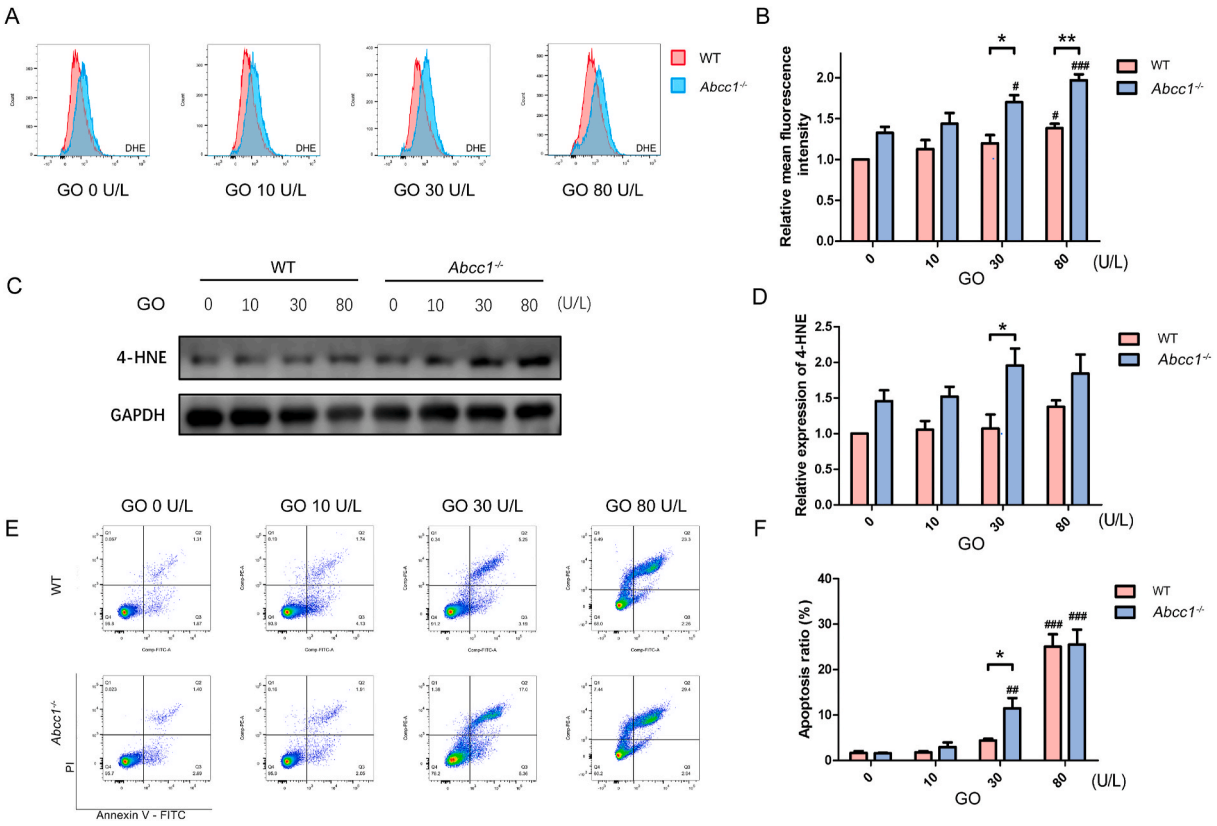

Fig. 5. Compared with WT ECs, *Abcc1*$^{-/-}$ ECs suffer more severe oxidative stress damage. (A) Representative images showing the fluorescence intensities of DHE in GO treated WT and *Abcc1*$^{-/-}$ cells. (B) Bar graph showing the relative mean fluorescence intensities of GO treated WT and *Abcc1*$^{-/-}$ cells (n = 3 for each group). (C) Western blot analysis of 4-HNE expression in GO treated WT and *Abcc1*$^{-/-}$ cells. (D) Bar graph showing the relative mean expression of 4-HNE in GO treated WT and *Abcc1*$^{-/-}$ cells (n = 3 for each group). (E) Annexin V/PI staining and flow cytometry analysis of apoptosis in GO treated WT and *Abcc1*$^{-/-}$ cells. (F) Bar graph showing the percentages of apoptotic WT and *Abcc1*$^{-/-}$ cells (n = 3 for each group). Comparation between the GO treated groups and the 0 U/L control group among the same genotype: #P < 0.05, ##P < 0.01, ###P < 0.001. Comparison of different genotypes under the same experimental conditions: *P < 0.05, **P < 0.01.

compared with those in the GO treated groups, ROS production, 4-HNE accumulation and apoptosis in the WT and *Abcc1*$^{-/-}$ cells were ameliorated to different extents after NAC administration (Fig. 8A–F). This result indicated that NAC may compensate for the increase in antioxidant capacity of *Abcc1*$^{-/-}$ cells.

4. Discussion

In this study, we established an *Abcc1* knockout mouse model to explore the pathophysiological role of ABCC1 in the inner ear and the mechanism underlying ABCC1 mutation-associated hearing impairment. After 5 months of observation, we detected no noticeable pathological changes in auditory function or inner ear morphology in the *Abcc1*$^{-/-}$ mice (Fig. 2). After low-intensity noise exposure for 7 days, the ABR thresholds of both the WT and *Abcc1*$^{-/-}$ mice were elevated. Fourteen days after recovery, the ABR threshold of the WT mice declined to baseline, yet there was no improvement in the ABR threshold of the *Abcc1*$^{-/-}$ mice (Fig. 3). In addition, morphological damage, including vessel leakage in the StV, OHC loss and ribbon decreases in organ of Corti, was detected in *Abcc1*$^{-/-}$ mice after noise exposure, and the levels of ROS and 4-HNE were significantly increased in the cochleae of *Abcc1*$^{-/-}$ mice (Fig. 4). Furthermore, we found that primary cultured *Abcc1*$^{-/-}$ StV ECs were more susceptible to GO-induced oxidative stress damage than WT ECs, and the GSH antioxidant system was compromised in the *Abcc1*$^{-/-}$ ECs (Figs. 5 and 6).

It was reported that mice with knockout of ABCB1, the other ABC transporter expressed in the blood-labyrinth barrier, exhibited normal hearing, while they were more susceptible to anticancer drug-induced ototoxicity [23]. Similarly, *Abcc1*$^{-/-}$ mice did not exhibit an abnormal phenotype under normal condition. However, *Abcc1*$^{-/-}$ mice were more susceptible to noise induced hearing loss. It indicated that environmental factors may be involved in ABCC1 mutation induced hearing loss.

As a transporter with multiple physiological functions, ABCC1 can not only mediate ATP-dependent drug efflux from cells but also transport exogenous and endogenous toxic metabolites and regulate the leukotriene-mediated inflammatory response [24]. ABCC1 can mediate the efflux of GSH, which is the most potent endogenous antioxidant, GSSG and oxidized metabolites from cells to modulate redox biology in various tissues and cells [25–27]. Under conditions of endogenous oxidative stress, the accumulation of GSSG and other GSH-conjugated metabolites in ABCC1 mutant cells can lead to cell damage [28,29]. Some studies have shown that overexpression of ABCC1 sensitized multidrug-resistant cancer cells to ferroptosis through its capacity to generate GSH efflux [30,31]. In this study, increased free radical production and lipid peroxide accumulation were observed in the cochleae of *Abcc1*$^{-/-}$ mice after noise exposure. It may be due to efflux disorder of GSH-conjugated oxidized metabolites in *Abcc1*$^{-/-}$ mice.

Low-intensity noise causes metabolic damage by interfering with metabolism in the cochlea, which is mainly caused by noise-induced oxidative stress damage [32]. ABCC1 is mainly expressed in the microvascular ECs of the StV, which construct the blood-labyrinth barrier. It indicated that in the cochleae of *Abcc1*$^{-/-}$ mice, ABCC1 was deleted in the microvascular ECs of the StV. Our results showed that after noise exposure, blood vessel integrity in the StV of *Abcc1*$^{-/-}$ mice was compromised, which may be caused by excessive oxidative stress damage. In addition to the StV, *Abcc1*$^{-/-}$ mice also exhibited ROS overaccumulation in the organ of Corti. It has been reported that the survival

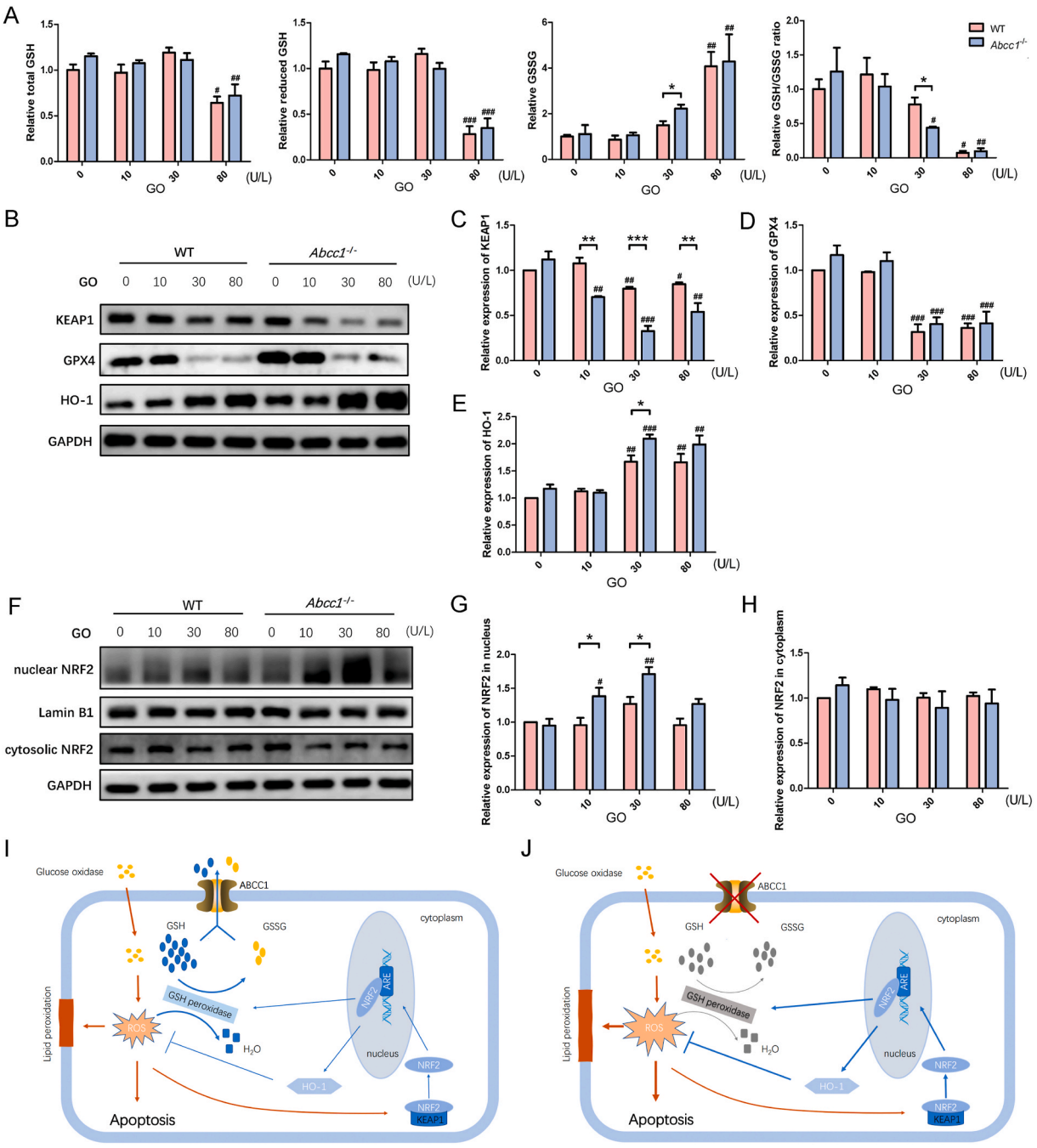

Fig. 6. The antioxidant capacity of *Abcc1*$^{-/-}$ cells was compromised. (A) Bar graphs showing the relative mean levels of total GSH, reduced GSH, and GSSG and the GSH/GSSG ratio in WT and *Abcc1*$^{-/-}$ cells after 0, 10, 30 and 80 U/L GO treatment for 4 h. (B) Western blot analysis of the expression of KEAP1, GPX4 and HO-1 in GO treated WT and *Abcc1*$^{-/-}$ cells. GAPDH served as a loading control for KEAP1, GPX4 and HO-1. (*C*–E) Bar graphs showing the relative mean expression of KEAP1, GPX4 and HO-1. (F) Western blot analysis of the expression of nuclear and cytosolic NRF2 in GO treated WT and *Abcc1*$^{-/-}$ cells. Lamin B1 served as a loading control for nuclear NRF2. GAPDH served as a loading control for cytosolic NRF2. (G–H) Bar graphs showing the relative mean expression of nuclear and cytosolic NRF2. Comparation between the GO treated groups and the 0 U/L control group among the same genotype: #P < 0.05, ##P < 0.01, ###P < 0.001. Comparison of different genotypes under the same experimental conditions: *P < 0.05, **P < 0.01, ***P < 0.001. (I) Schematic representation of the oxidative stress response induced by glucose oxidase in WT cells. (J) Schematic representation of the oxidative stress response induced by glucose oxidase in cells following ABCC1 deletion.

of hair cells in organ of Corti relies on the normal morphology and function of the StV [33]. Therefore, damage to the organ of Corti, including OHC loss and decreased ribbons, may be secondary to StV damage in *Abcc1*$^{-/-}$ mice.

Endothelial cells are sensitive to oxidative stress. ABCC1 is expressed in vascular ECs and can protect against oxidative stress damage by preventing intracellular GSSG accumulation [34,35]. The blood-labyrinth is a physical barrier between the blood and the interstitial space in the cochlea and plays a crucial role in the maintenance of cochlear homeostasis [36,37]. Destruction of the blood-labyrinth barrier is closely related to many hearing disorders, including autoimmune inner ear diseases, age-related hearing loss and noise-induced hearing loss [38–41]. Based on the localization of ABCC1, we used primary cultures of StV microvascular ECs to further investigate the specific role of ABCC1 in the inner ear. Our results demonstrated that *Abcc1*$^{-/-}$ cells were more susceptible to GO-induced oxidative stress

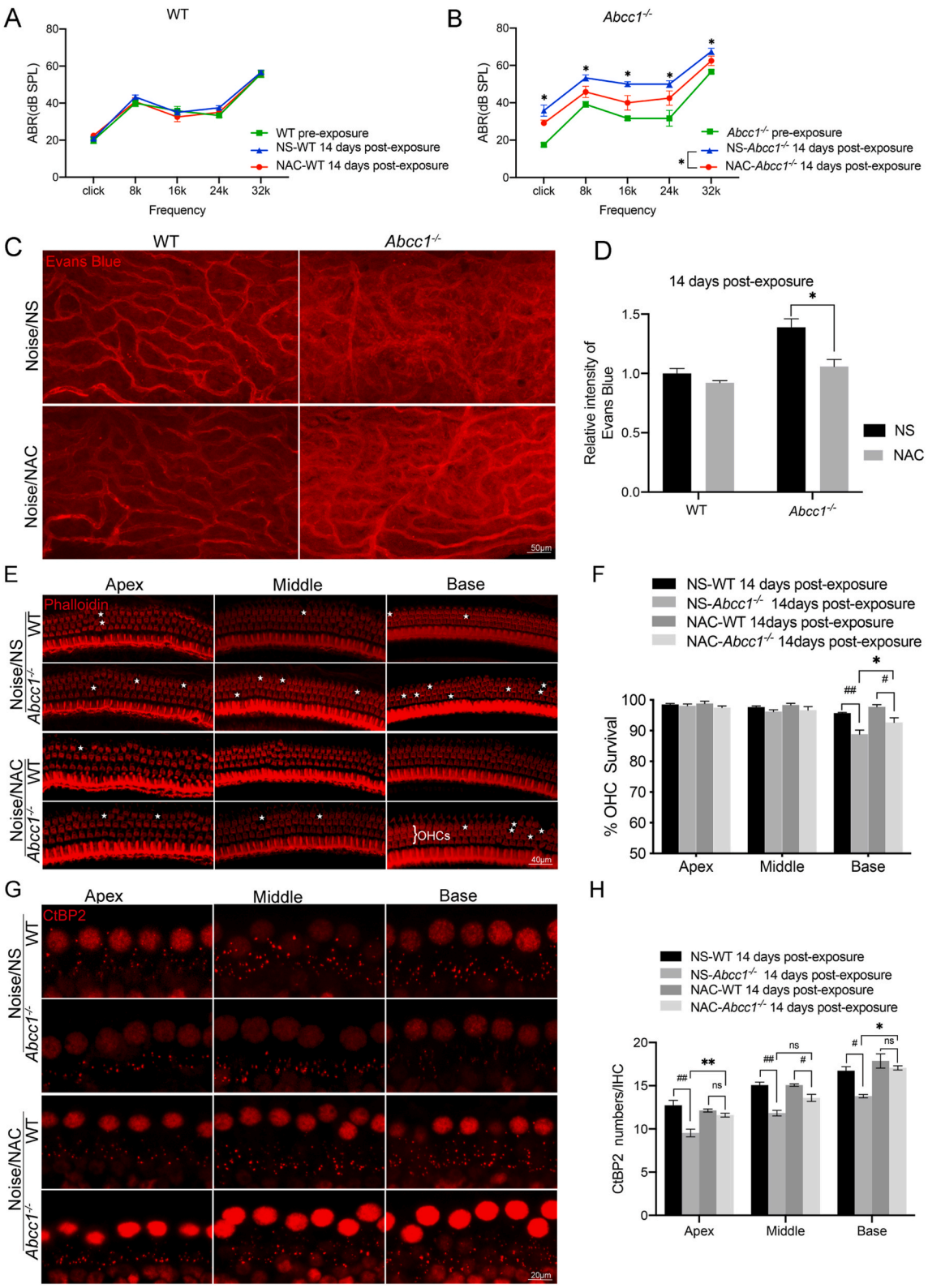

Fig. 7. NAC alleviated noise-induced permanent hearing loss in *Abcc1*$^{-/-}$ mice. (A–B) ABR thresholds of WT mice and *Abcc1*$^{-/-}$ mice treated with NAC before and 14 days after noise exposure. (C) Confocal images of microvessels in the StV after EB infusion. Scale bar: 50 μm. (D) Bar graph of the relative fluorescence intensity of EB (n = 3 for each group). (E) Confocal images of OHCs in WT and *Abcc1*$^{-/-}$ mice treated with NS or NAC 14 days after noise exposure. White pentagrams indicate the absence of hair cells. Scale bar: 50 μm. (F) Percentage of OHC loss at different cochlear locations in WT and *Abcc1*$^{-/-}$ mice treated with NS or NAC (n = 3 for each group). (G) Confocal images of ribbons at different cochlear locations in wild-type and *Abcc1*$^{-/-}$ mice treated with NS or NAC 14 days after noise exposure. Scale bar: 20 μm. (H) The number of ribbons per IHC was quantified in WT and *Abcc1*$^{-/-}$ mice subjected to NS or NAC administration 14 days after noise exposure (n = 3 for each group). Comparison of the NS and NAC groups among the same genotype 14 days post-exposure: *P < 0.05, **P < 0.01. Comparison of the WT and *Abcc1*$^{-/-}$ groups under same treatment condition 14 days post-exposure: #P < 0.05, ##P < 0.01.

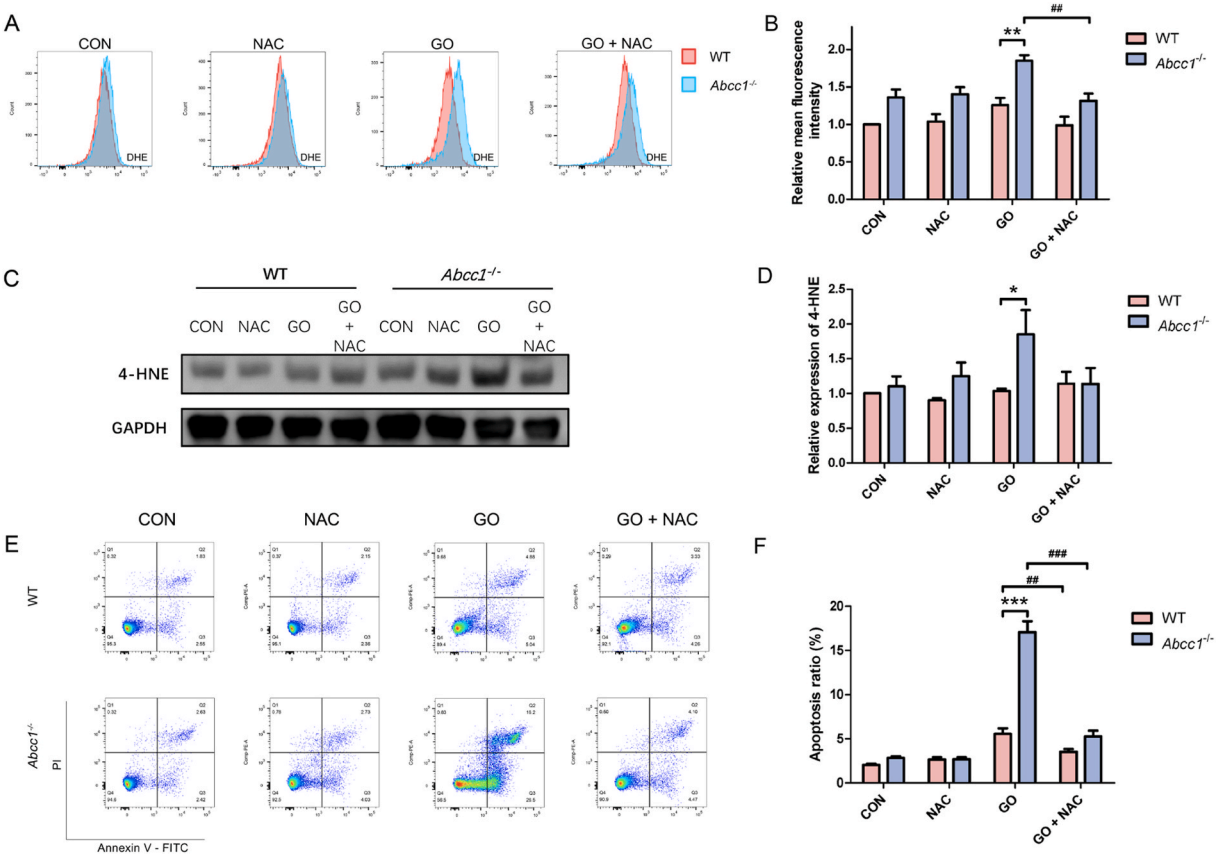

Fig. 8. NAC mitigated oxidative damage in both WT and *Abcc1*$^{-/-}$ ECs. (A) Representative images showing the fluorescence intensities of DHE in 0 U/L GO, 10 mM NAC, 30 U/L GO or 30 U/L GO + 10 mM NAC treated WT and *Abcc1*$^{-/-}$ cells. (B) The bar graph of the relative mean fluorescence intensities of WT and *Abcc1*$^{-/-}$ cells with various treatment. (C) Western blot analysis of 4-HNE expression in 0 U/L GO, 10 mM NAC, 30 U/L GO or 30 U/L GO + 10 mM NAC treated WT and *Abcc1*$^{-/-}$ cells. (D) The bar graph showing the relative mean expression of 4-HNE in WT and *Abcc1*$^{-/-}$ cells subjected to various treatments. (E) Annexin V/PI staining and flow cytometry analysis of apoptosis in 0 U/L GO, 10 mM NAC, 30 U/L GO or 30 U/L GO + 10 mM NAC treated WT and *Abcc1*$^{-/-}$ cells. (F) Bar graph showing the percentages of apoptotic WT and *Abcc1*$^{-/-}$ cells after treatment with 0 U/L GO, 10 mM NAC, 30 U/L GO or 30 U/L GO + 10 mM NAC. Comparison of different treatment groups with the same genotype: ##P < 0.01, ###P < 0.001. Comparison of different genotypes under the same experimental conditions: *P < 0.05, **P < 0.01, ***P < 0.001.

damage. This may be because ABCC1 knockout blocked the efflux of GSSG and decreased the GSH/GSSG ratio, leading to disturbance of the GSH antioxidant system in *Abcc1*$^{-/-}$ cells. The NRF2 signaling pathway was more active in *Abcc1*$^{-/-}$ ECs. This may partially compensate for the antioxidant capacity of *Abcc1*$^{-/-}$ ECs under low-dose oxidative stress. Overall, ABCC1 deficiency compromised the antioxidant capacity of StV microvascular ECs (Fig. 6I and J).

Based on these results, we further investigated whether exogenous antioxidants could protect *Abcc1*$^{-/-}$ mice against oxidative stress. Administration of NAC, a glutathione analog, significantly protected the morphology and function of the inner ear in *Abcc1*$^{-/-}$ mice. In addition, in vitro experiments showed that NAC significantly mitigated GO-induced oxidative damage in *Abcc1*$^{-/-}$ ECs. This result indicated that NAC administration may serve as an effective and convenient avenue for the prevention and intervention of oxidative damage-induced hearing loss caused by *Abcc1* gene defects.

In conclusion, we investigated the potential pathogenesis of ABCC1 mutation-associated hearing impairment by using an *Abcc1* knockout mouse model. We demonstrated that *Abcc1* knockdown may compromise the antioxidant system of GSH, increasing the susceptibility of the cochleae of *Abcc1*$^{-/-}$ mice to oxidative stress damage. NAC may be a therapeutic agent for protecting the auditory function of ABCC1 mutant patients from oxidative stress damage. Our work may provide new insights for studying the pathogenesis and treatment strategies of hereditary, late-onset, progressive sensorineural hearing loss.

CRediT authorship contribution statement

Jing Liu: Writing – original draft, Resources, Methodology, Investigation, Formal analysis, Data curation, Conceptualization. **Yijiang Bai:** Writing – original draft, Visualization, Resources, Methodology, Investigation, Formal analysis, Data curation, Conceptualization. **Yong Feng:** Writing – review & editing, Validation, Funding acquisition. **Xianlin Liu:** Visualization, Investigation. **Bo Pang:** Visualization, Investigation. **Shuai Zhang:** Visualization, Investigation. **Mengzhu Jiang:** Visualization, Investigation. **Anhai Chen:** Visualization, Investigation. **Huping Huang:** Visualization, Investigation. **Yongjia Chen:** Visualization, Investigation. **Jie Ling:** Writing – review & editing, Supervision, Project administration, Funding acquisition, Conceptualization. **Lingyun Mei:** Writing – review & editing, Supervision, Project administration, Funding acquisition, Conceptualization.

Declaration of competing interest

The authors declare that they have no known competing financial interests or personal relationships that could have appeared to influence the work reported in this paper.

Data availability

Data will be made available on request.

Acknowledgments

This work was supported by the National Natural Science Foundation of China (Grant No. 82171154, 81873705, 82101233).

Appendix A. Supplementary data

Supplementary data to this article can be found online at https://doi.org/10.1016/j.redox.2024.103218.

References

[1] L. Jiang, D. Wang, Y. He, Y. Shu, Advances in gene therapy hold promise for treating hereditary hearing loss, Mol. Ther. 31 (4) (2023) 934–950.
[2] R.L. Alford, K.S. Arnos, M. Fox, et al., American College of Medical Genetics and Genomics guideline for the clinical evaluation and etiologic diagnosis of hearing loss, Genet. Med. 16 (4) (2014) 347–355.
[3] A.M. Sheffield, R.J.H. Smith, The epidemiology of deafness, Cold. Spring. Harb. Perspect. Med 9 (9) (2019) a033258.
[4] M. Li, L. Mei, C. He, et al., Extrusion pump ABCC1 was first linked with nonsyndromic hearing loss in humans by stepwise genetic analysis, Genet. Med. 21 (12) (2019) 2744–2754.
[5] S.P. Cole, Targeting multidrug resistance protein 1 (MRP1, ABCC1): past, present, and future, Annu. Rev. Pharmacol. Toxicol. 54 (2014) 95–117.
[6] K.M. Hanssen, M. Haber, J.I. Fletcher, Targeting multidrug resistance-associated protein 1 (MRP1)-expressing cancers: beyond pharmacological inhibition, Drug Resist. Updates 59 (2021) 100795.
[7] S.P. Cole, Multidrug resistance protein 1 (MRP1, ABCC1), a "multitasking" ATP-binding cassette (ABC) transporter, J. Biol. Chem. 289 (45) (2014) 30880–30888.
[8] D.F. Leite, J. Echevarria-Lima, J.B. Calixto, et al., Multidrug resistance related protein (ABCC1) and its role on nitrite production by the murine macrophage cell line RAW 264.7, Biochem. Pharmacol. 73 (5) (2007) 665–674.
[9] E.M. Leslie, Arsenic-glutathione conjugate transport by the human multidrug resistance proteins (MRPs/ABCCs), J. Inorg. Biochem. 108 (2012) 141–149.
[10] D.M. Klein, S.H. Wright, N.J. Cherrington, Localization of multidrug resistance-associated proteins along the blood-testis barrier in rat, macaque, and human testis, Drug Metab. Dispos. 42 (1) (2014) 89–93.
[11] L. Tupova, B. Hirschmugl, S. Sucha, et al., Interplay of drug transporters P-glycoprotein (MDR1), MRP1, OATP1A2 and OATP1B3 in passage of maraviroc across human placenta, Biomed. Pharmacother. 129 (2020) 110506.
[12] L.F.M. Verscheijden, A.C. van Hattem, J.C.L.M. Pertijs, et al., Developmental patterns in human blood-brain barrier and blood-cerebrospinal fluid barrier ABC drug transporter expression, Histochem. Cell Biol. 154 (3) (2020) 265–273.
[13] T. Saito, Z.J. Zhang, M. Tokuriki, et al., Expression of multidrug resistance protein 1 (MRP1) in the rat cochlea with special reference to the blood-inner ear barrier, Brain Res. 895 (1–2) (2001) 253–257.
[14] J.D. Johns, S.M. Adadey, M. Hoa, The role of the stria vascularis in neglected otologic disease, Hear. Res. 428 (2023) 108682.
[15] J. Zielonka, M. Zielonka, A. Sikora, et al., Global profiling of reactive oxygen and nitrogen species in biological systems: high-throughput real-time analyses, J. Biol. Chem. 287 (5) (2012) 2984–2995.
[16] L. Neng, W. Zhang, A. Hassan, et al., Isolation and culture of ECs, pericytes and perivascular resident macrophage-like melanocytes from the young mouse ear, Nat. Protoc. 8 (4) (2013) 709–720.
[17] W.J. Jiang, Z. Zhou, Y.P. Wang, et al., PGC-1α affects cochlear pericytes migration in noise-exposed mice, Biochem. Biophys. Res. Commun. 687 (2023) 149172.
[18] T. Münzel, A. Daiber, S. Steven, et al., Effects of noise on vascular function, oxidative stress, and inflammation: mechanistic insight from studies in mice, Eur. Heart J. 38 (37) (2017) 2838–2849.
[19] H.Y. Jiang, Y. Yang, Y.Y. Zhang, et al., The dual role of poly(ADP-ribose) polymerase-1 in modulating parthanatos and autophagy under oxidative stress in rat cochlear marginal cells of the stria vascularis, Redox Biol. 14 (2018) 361–370.
[20] M.J. Ferreira, T.A. Rodrigues, A.G. Pedrosa, et al., Glutathione and peroxisome redox homeostasis, Redox Biol. 67 (2023) 102917.
[21] Q. Zhang, J. Liu, H. Duan, et al., Activation of Nrf2/HO-1 signaling: an important molecular mechanism of herbal medicine in the treatment of atherosclerosis *via* the protection of vascular endothelial cells from oxidative stress, J. Adv. Res. 34 (2021) 43–63.
[22] M. Guerini, G. Condrò, V. Friuli, L. Maggi, P. Perugini, N-Acetylcysteine (NAC) and its role in clinical practice management of cystic fibrosis (CF): a review, Pharmaceuticals 15 (2) (2022) 217.
[23] Z.J. Zhang, T. Saito, Y. Kimura, et al., Disruption of mdr1a p-glycoprotein gene results in dysfunction of blood-inner ear barrier in mice, Brain Res. 852 (1) (2000) 116–126.
[24] E.E. Smith, G. Conseil, S.P.C. Cole, Conserved amino acids in the region connecting membrane spanning domain 1 to nucleotide binding domain 1 are essential for expression of the MRP1 (ABCC1) transporter, PLoS One 16 (2) (2021) e0246727.
[25] S. Granitzer, I. Ellinger, R. Khan, et al., In vitro function and in situ localization of Multidrug Resistance-associated Protein (MRP)1 (ABCC1) suggest a protective role against methyl mercury-induced oxidative stress in the human placenta, Arch. Toxicol. 94 (11) (2020) 3799–3817.
[26] J. Hirrlinger, J. König, D. Keppler, et al., The multidrug resistance protein MRP1 mediates the release of glutathione disulfide from rat astrocytes during oxidative stress, J. Neurochem. 76 (2) (2001) 627–636.
[27] I. Ellison, J.P. Richie Jr., Mechanisms of glutathione disulfide efflux from erythrocytes, Biochem. Pharmacol. 83 (1) (2012) 164–169.
[28] N. Ballatori, S.M. Krance, S. Notenboom, et al., Glutathione dysregulation and the etiology and progression of human diseases, Biol. Chem. 390 (3) (2009) 191–214.
[29] R.M. Laberge, J. Karwatsky, M.C. Lincoln, et al., Modulation of GSH levels in ABCC1 expressing tumor cells triggers apoptosis through oxidative stress, Biochem. Pharmacol. 73 (11) (2007) 1727–1737.
[30] J.Y. Cao, A. Poddar, L. Magtanong, et al., A genome-wide haploid genetic screen identifies regulators of glutathione abundance and ferroptosis sensitivity, Cell Rep. 26 (6) (2019) 1544–1556.e8.
[31] I. de Souza, L.K.S. Monteiro, C.B. Guedes, et al., High levels of NRF2 sensitize temozolomide-resistant glioblastoma cells to ferroptosis via ABCC1/MRP1 upregulation, Cell Death Dis. 13 (7) (2022) 591.
[32] W.J. Tan, P.R. Thorne, S.M. Vlajkovic, Characterisation of cochlear inflammation in mice following acute and chronic noise exposure, Histochem. Cell Biol. 146 (2) (2016) 219–230.
[33] H Liu, Y Li, L Chen, et al., Organ of Corti and stria vascularis: is there an interdependence for survival? PLoS One 11 (12) (2016) e0168953.
[34] Y.L. Zhang, J. Wang, Z.N. Zhang, et al., The relationship between amyloid-beta and brain capillary ECs in Alzheimer's disease, Neural. Regen. Res. 17 (11) (2022) 2355–2363.
[35] K. Takahashi, T. Shibata, T. Oba, et al., Multidrug-resistance-associated protein plays a protective role in menadione-induced oxidative stress in ECs, Life Sci. 84 (7–8) (2009) 211–217.
[36] X. Shi, Pathophysiology of the cochlear intrastrial fluid-blood barrier, Hear. Res. 338 (2016) 52–63.
[37] S. Nyberg, N.J. Abbott, X. Shi, et al., Delivery of therapeutics to the inner ear: the challenge of the blood-labyrinth barrier, Sci. Transl. Med. 11 (482) (2019) eaao0935.
[38] D.W. Lin, D.R. Trune, Breakdown of stria vascularis blood-labyrinth barrier in C3H/lpr autoimmune disease mice, Otolaryngol. Head Neck Surg. 117 (1997) 530–534.
[39] W. Zhang, M. Dai, A. Fridberger, et al., Perivascular-resident macrophage-like melanocytes in the inner ear are essential for the integrity of the intrastrial fluid-blood barrier, Proc. Natl. Acad. Sci. U.S.A. 109 (26) (2012) 10388–10393.
[40] M.A. Gratton, B.A. Schulte, N.M. Smythe, Quantification of the stria vascularis and strial capillary areas in quiet-reared young and aged gerbils, Hear. Res. 114 (1997) 1–9.
[41] X. Shi, Cochlear pericyte responses to acoustic trauma and the involvement of hypoxia-inducible factor-1alpha and vascular endothelial growth factor, Am. J. Pathol. 174 (2009) 1692–1704.